

DIPPAS: A Deep Image Prior PRNU Anonymization Scheme

Francesco Picetti, Sara Mandelli, Paolo Bestagini, *Member, IEEE*, Vincenzo Lipari, and Stefano Tubaro, *Senior Member, IEEE*

Abstract—Source device identification is an important topic in image forensics since it allows to trace back the origin of an image. Its forensics counter-part is source device anonymization, that is, to mask any trace on the image that can be useful for identifying the source device. A typical trace exploited for source device identification is the Photo Response Non-Uniformity (PRNU), a noise pattern left by the device on the acquired images. In this paper, we devise a methodology for suppressing such a trace from natural images without significant impact on image quality. Specifically, we turn PRNU anonymization into an optimization problem in a Deep Image Prior (DIP) framework. In a nutshell, a Convolutional Neural Network (CNN) acts as generator and returns an image that is anonymized with respect to the source PRNU, still maintaining high visual quality. With respect to widely-adopted deep learning paradigms, our proposed CNN is not trained on a set of input-target pairs of images. Instead, it is optimized to reconstruct the PRNU-free image from the original image under analysis itself. This makes the approach particularly suitable in scenarios where large heterogeneous databases are analyzed and prevents any problem due to lack of generalization. Through numerical examples on publicly available datasets, we prove our methodology to be effective compared to state-of-the-art techniques.

I. INTRODUCTION

Source device identification is a well-studied problem in the multimedia forensics community [1], [2], [3], [4]. Indeed, identifying the source camera of an image helps to trace its origin and verifying its integrity. Many state-of-the-art techniques tackle this problem by relying on Photo Response Non-Uniformity (PRNU), which is a unique characteristic noise pattern left by the device on each acquired content [1]. Given a query image and a candidate device, it is possible to infer whether the image was shot by the device with a cross-correlation test between a noise trace extracted from the image and the device PRNU [5].

Despite the effort put into developing robust PRNU-based source attribution techniques, the forensic community has also focused on studying the possibility of removing PRNU traces from images. On one hand, determining at which level PRNU can be actually removed is essential to study the robustness of PRNU-based forensic detectors, and possibly improve them. On the other hand, when privacy is a concern, being able to link a picture to its owner is clearly undesirable. As an example, photojournalists carrying out legit investigations may prefer to anonymize their shots in order to avoid being threatened.

For these reasons, counter-forensic methods that enable deleting or reducing PRNU traces from images have been proposed in the literature. We subdivide the developed techniques into two families. The first family requires the knowledge of the PRNU pattern to be deleted, and we refer to them as PRNU-aware methods. This is the case of [6], [7], [8], which propose different iterative solutions to delete a known PRNU from a given picture. Specifically, [6] proposes an adaptive PRNU-based image denoising, removing an estimate of the PRNU from each image. Authors of [7] estimate the best subtraction weight that minimizes the cross-correlation between the PRNU and the trace extracted from the image to be anonymized. Recently, [8] applies a Convolutional Neural Network (CNN), which exploits the source PRNU to hinder its traces from a query image. The network is used as a parametric operator, which iteratively overfits the given pair of image and PRNU, imposing a minimization of their correlation.

The second family of methods works by blindly modifying pixel values in order to make the underlying PRNU unrecognizable. For instance, [9] shows that multiple image denoising steps can help attenuating the PRNU, even though this may not be enough to completely hinder its traces from images [10]. Alternatively, [11] applies seam-carving to change pixel locations, and [12] exploits patch-match techniques to scramble pixel positions. More recently, [13] proposes an inpainting-based method which deletes and reconstructs image pixels such that final images are anonymized with respect to their source PRNU.

In this manuscript, we propose an image anonymization tool leveraging a CNN. Specifically, given an image to be anonymized and a reference PRNU trace to be removed, the proposed network deletes traces of such PRNU from the image. Differently from most CNN works, the proposed network does not need a training step. In fact, the proposed CNN exploits the Deep Image Prior (DIP) paradigm [14], thus acting as a framework to solve an inverse problem: estimate the PRNU-free image from the picture under analysis and a reference PRNU trace. The proposed CNN takes a random noise realization as input and iterates until it is capable of generating a PRNU-free representation of a selected picture. The analyst can decide when to stop CNN iterations by simply checking the trade-off between the quality of the generated image and the reached anonymization level.

In this context, image anonymization can be interpreted as an inverse problem with prior information. The prior is the network itself. Thus, the architecture plays a key role in the optimization routine. In order to capture the deep features from

F. Picetti, S. Mandelli, P. Bestagini, V. Lipari, and S. Tubaro are with the Dipartimento di Elettronica, Informazione e Bioingegneria, Politecnico di Milano, Milano 20133, Italy (e-mail: name.surname@polimi.it).

the analyzed picture, we adopt a multiresolution U-Net design [15], which has been proposed to improve the original U-Net [16] for multimodal medical image segmentation where the targets of interest have different shapes and scales.

The developed anonymization scheme is validated on 1200 color images of the well known Dresden Image Database [17] and 600 color images of the Vision Source Identification Dataset [18]. In doing so, we address the anonymization problem on both uncompressed images (i.e., images selected from Dresden dataset) and JPEG-compressed images (i.e., images from both Dresden and Vision datasets). For the sake of comparison with state-of-the-art techniques, we test our methodology both when an estimate of the device PRNU is available (i.e., in a PRNU-aware scenario) and when the device PRNU can be estimated only from the query image itself (i.e., in a PRNU-blind scenario). Results show that the proposed technique actually hinders PRNU-based detectors, especially when the actual device PRNU is available.

The rest of the paper is organized as follows. In Section II, we provide the reader with the background concepts useful for understanding the core of the proposed methodology. In Section III, we present the details of the proposed scheme. In particular, we first define the inverse problem we aim at solving, then we devise a processing pipeline to obtain the target PRNU-free image. Finally, we describe the architecture design along with the optimization strategies. In Section IV, we describe the considered experimental setup. In Section VI, we report all the numerical results achieved with our experiments. Eventually, in Section VI we draw our conclusions.

II. BACKGROUND AND PROBLEM STATEMENT

In this section, we introduce some background concepts useful to understand the rest of the paper. First, we introduce Photo Response Non-Uniformity (PRNU) and its use for in source device identification. Then, we present the adopted methodology known as Deep Image Prior (DIP) [14], which has been recently proposed as a paradigm to solve diverse inverse problems like image denoising. Eventually, we provide the formulation of the source device anonymization problem faced in this paper.

A. Photo Response Non-Uniformity

Photo Response Non-Uniformity (PRNU) is a characteristic noise fingerprint introduced in all images acquired by a device. Specifically, the PRNU \mathbf{K} has the form of a zero-mean pixel-wise multiplicative noise. According to the well-known model proposed in [1], [2], a generic image \mathbf{I} shot by a digital device can be described as

$$\mathbf{I} = \mathbf{I}_0 (1 + \gamma \mathbf{K}) + \Theta \quad (1)$$

where \mathbf{I}_0 is the sensor output in the absence of noise, γ is the weight of the PRNU contribution, and Θ includes all the additional independent random noise components. The PRNU \mathbf{K} can be estimated by collecting a set of images shot by the device, following the method proposed in [1], [2].

PRNU \mathbf{K} is commonly used to solve source device identification problem, that is, given a query image \mathbf{I} and a candidate

device, understanding if the device shot that image or not. One way to solve the problem is to compute the Normalized Cross-Correlation (NCC) between a noise residual \mathbf{W} [2] extracted from the query image \mathbf{I} and the PRNU \mathbf{K} of the candidate device, pixel-wise scaled by \mathbf{I} . Formally, NCC is defined as

$$\text{NCC}(\mathbf{W}, \mathbf{IK}) = \frac{\text{corr}(\mathbf{W}, \mathbf{IK})}{\|\mathbf{W}\|_F \cdot \|\mathbf{IK}\|_F}, \quad (2)$$

being $\|\cdot\|_F$ the Frobenius norm. If $\text{NCC}(\mathbf{W}, \mathbf{IK})$ is greater than a predefined threshold, the image can be attributed to the device with a certain confidence.

B. Deep Image Prior (DIP)

A generic image restoration problem is usually solved through the minimization of an objective function of the form

$$J(\mathbf{x}) = E(\mathbf{x}; \mathbf{I}) + \lambda R(\mathbf{x}), \quad (3)$$

where $E(\mathbf{x}; \mathbf{I})$ is a task-dependent misfit function conditioned by the (corrupted) input image \mathbf{I} and $R(\mathbf{x})$ is a regularization term designed to tackle the ill-posedness and ill-conditioning of the inverse problem. To avoid confusion with the rest of notation used in the paper, we refer at \mathbf{x} as a generic image which the cost function is evaluated for. λ is a weight setting the trade-off between honoring the data and imposing the desired a-priori features [19]. The restored image $\hat{\mathbf{x}}$ is then obtained as

$$\hat{\mathbf{x}} = \arg \min_{\mathbf{x}} J(\mathbf{x}). \quad (4)$$

The data misfit $E(\mathbf{x}; \mathbf{I})$ is usually quite simple to devise, and it depends on the desired task. The design of a regularization term $R(\mathbf{x})$ can be challenging because it should capture the features of the desired image. In the past years, the imaging community has focused its efforts on designing regularizers able to enforce a-priori knowledge on the image to be retrieved. Among them, Tikhonov regularization [20] privileges minimum energy solutions and Total Variation (TV) [21] privileges flat-zones solutions. Lately, more elaborated regularizers have been based on the idea that the image can be conveniently represented in a transformed domain such as the Fourier domain, or using Wavelet-based representations [22], Curvelets [23], Contourlets [24], and Shearlets [25].

Deep Image Prior (DIP) has been proposed as an alternative solution with respect to standard regularization [14]. The objective function to minimize is recast as

$$J(\phi) = E(\mathbf{x}; \mathbf{I}) = E(f_\phi(\mathbf{z}); \mathbf{I}), \quad (5)$$

where $f_\phi(\cdot)$ is a CNN represented as a parametric non linear function, ϕ are the parameters of this function (i.e., the weights of the CNN), and \mathbf{z} is a random noise realization. The value $f_\phi(\mathbf{z})$ is associated with the output image to the network, thus it is related to a random noise realization \mathbf{z} and to the CNN parameters ϕ . Notice that there is not an explicit regularization term: the CNN architecture itself plays the role of the prior. Through its convolutional layers, the CNN captures the inner structure and self-similarities of the desired uncorrupted image from the input corrupted one, and constraints the solution space.

In other words, instead of minimizing the objective function in the space of the image as in (4), DIP performs the search in the space of the CNN parameters ϕ and this dramatically changes the shape of the objective function, driving the solution to honor both the data misfit and the deep features captured on the corrupted input image. The restored image is then obtained as

$$\hat{\mathbf{x}} = f_{\hat{\phi}}(\mathbf{z}) \quad (6)$$

where

$$\hat{\phi} = \arg \min_{\phi} J(\phi). \quad (7)$$

It is worth noticing that the CNN optimization is not performed aiming at reconstructing a target image starting from a ground truth image. Indeed, the DIP method does not require a specifically designed set of data for training. Even though the result is the output of a CNN, DIP is not a typical deep learning paradigm.

For the specific case of image denoising, the DIP objective function presented in (5) is customary set to the ℓ_2 distance between the output image to the CNN for a given combination of noise realization \mathbf{z} and network parameters ϕ , defined as $f_{\phi}(\mathbf{z})$, and the input image \mathbf{I} [26], [27], [28]. For the sake of notation, from now on we refer to the CNN output image $f_{\phi}(\mathbf{z})$ as \mathbf{I}_{ϕ} . Therefore, (5) becomes

$$J(\phi) = \|\mathbf{I}_{\phi} - \mathbf{I}\|_2^2. \quad (8)$$

One may ask why a CNN that is designed to reconstruct a generic image should perform denoising while its goal is set to fit the input (noisy) image \mathbf{I} . The main reason is the different behaviour of signal and noise components throughout the iterative optimization [29]. If the minimization is led to convergence, the result will indeed fit the noisy image, but the authors of [14] have shown that parametrizing the optimization via the weights of a CNN generator distorts the search space so that in the minimization process the signal fits faster than the noise. Therefore, [14] proposes to perform denoising by early stopping the iterative minimization. For example, in a forensic scenario, the analyst can stop the optimization when some task-specific average metrics reach a desirable value.

C. Problem formulation

In this paper, we focus on the forensics counter-part of the source device identification problem, that is, performing source device anonymization. Specifically, given an image, we aim at hindering PRNU traces left on the image in order to make it impossible to associate the image with its original source device. Meanwhile, the visual quality of the anonymized image should not be compromised by the anonymization process. This translates into fulfilling two main goals:

- 1) the NCC between the anonymized image and the actual source PRNU should be lower than a predefined threshold;
- 2) the Peak-Signal-to-Noise-Ratio (PSNR) between the anonymized image and the original image should assume high values.

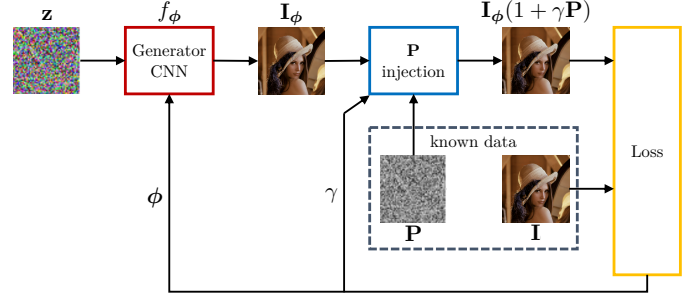


Fig. 1. Sketch of the proposed Deep Image Prior PRNU Anonymization Scheme (DIPPAS). The known data are the acquired image \mathbf{I} and the device fingerprint \mathbf{P} . During the inversion, the traces of \mathbf{P} are attenuated by injecting \mathbf{P} into the image \mathbf{I}_{ϕ} generated by the CNN. In the PRNU-aware setup, $\mathbf{P} = \mathbf{K}$; in the PRNU-blind setup, $\mathbf{P} = \mathbf{W}$, a noise residual extracted from \mathbf{I} [2].

To this purpose, we propose the Deep Image Prior PRNU Anonymization Scheme (DIPPAS), which is an anonymization method based on a DIP denoising scheme. In the following, we present the proposed strategy, discussing the main intuitions behind the approach.

III. PROPOSED METHODOLOGY

In this section, we illustrate all the details of the proposed approach. We start showing the theoretical DIP-based framework chosen for our specific problem. We then show how it is possible to obtain an anonymized picture using this framework. Given that DIP can return multiple versions of an anonymized image, we also show how to make the most out of this feature by assembling multiple images together to strengthen anonymization capability. Finally, we describe the employed CNN architecture.

A. DIP-based image anonymization

Considering the model (1) of a generic image \mathbf{I} acquired by a digital device, the anonymization task consists in estimating the ideal PRNU-free image \mathbf{I}_0 . Indeed, \mathbf{I}_0 is completely uncorrelated from the device PRNU and has a reasonably good visual quality. We achieve this goal by combining the DIP denoising paradigm of (8) with the PRNU-based image modeling proposed in (1). As previously reported, let us consider $\mathbf{I}_{\phi} = f_{\phi}(\mathbf{z})$ as the output of the CNN for a given parameter configuration ϕ and a noise realization \mathbf{z} . The functional to be minimized becomes

$$J(\phi) = \|\mathbf{I}_{\phi}(1 + \gamma\mathbf{P}) - \mathbf{I}\|_{\mathbb{F}}^2. \quad (9)$$

We define \mathbf{P} as the device fingerprint, that can be the estimated PRNU pattern (i.e., $\mathbf{P} = \mathbf{K}$) or the noise residual \mathbf{W} extracted from \mathbf{I} as suggested in [2].

The former situation is a PRNU-aware scenario (e.g., a user wants to anonymize its own photographs and knows the reference PRNU). In this case the proposed anonymization scheme makes use of the PRNU \mathbf{K} as the fingerprint \mathbf{P} , hence (9) becomes

$$J(\phi) = \|\mathbf{I}_{\phi}(1 + \gamma\mathbf{K}) - \mathbf{I}\|_{\mathbb{F}}^2. \quad (10)$$

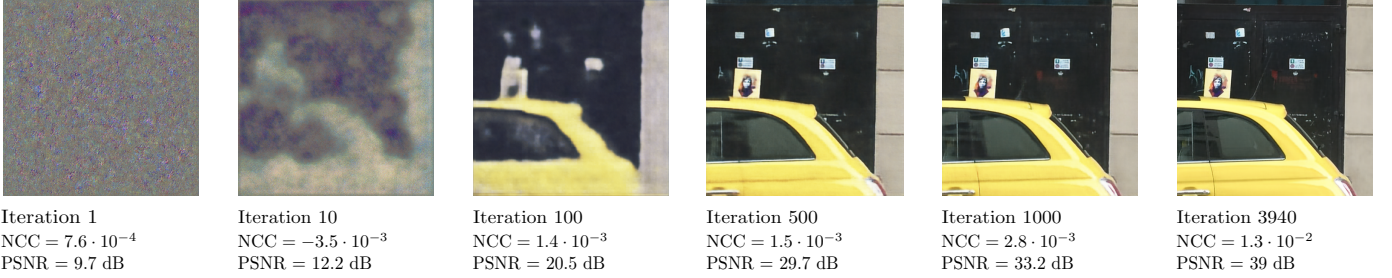


Fig. 2. DIPPAS inversion example: as iterations increase, the reconstructed image passes from a noisy behaviour (i.e., iteration 1) to a very similar copy of the original image.

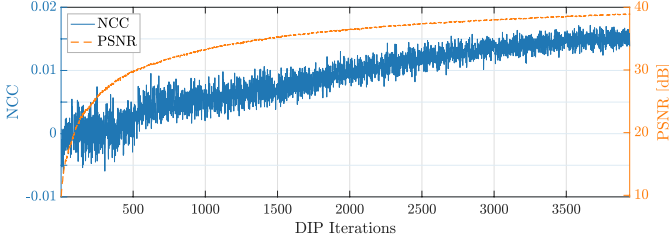


Fig. 3. NCC and PSNR behaviour as a function of DIPPAS iterations for the image depicted in Fig. 2 (best seen in colors).

The latter situation is a PRNU-blind scenario (e.g., a website wants to store anonymized images uploaded by users but each reference PRNU is not known at server side). In this case the fingerprint \mathbf{P} we inject in the inverse problem is the noise residual \mathbf{W} extracted from \mathbf{I} itself [2], hence (9) becomes

$$J(\phi) = \|\mathbf{I}_\phi(1 + \gamma\mathbf{W}) - \mathbf{I}\|_F^2. \quad (11)$$

Notice that the term $\mathbf{I}_\phi(1 + \gamma\mathbf{P})$ emulates the image modeling shown in (1) (correctly if $\mathbf{P} = \mathbf{K}$, approximately if $\mathbf{P} = \mathbf{W}$). The more $\mathbf{I}_\phi(1 + \gamma\mathbf{P})$ approaches \mathbf{I} in terms of Frobenius norm, the more \mathbf{I}_ϕ will reasonably represent a better estimate of the ideal PRNU-free image \mathbf{I}_0 , apart from independent random noise contributions. Given these premises, the estimated image \mathbf{I}_ϕ is a good candidate for the anonymization of the input image \mathbf{I} .

In a nutshell, the proposed strategy is depicted in Fig. 1. Starting from image \mathbf{I} , we extract the device noiseprint \mathbf{P} either in PRNU-aware or PRNU-blind scenario. Then, we generate the image \mathbf{I}_ϕ following the DIP paradigm, i.e., imposing the fingerprint-injected image $\mathbf{I}_\phi(1 + \gamma\mathbf{P})$ to be as similar as possible to the known image \mathbf{I} . By minimizing the functional (9), we estimate the anonymized image \mathbf{I}_ϕ .

B. Anonymized image generation process

The image generation pipeline is the following:

- 1) We normalize the input query image \mathbf{I} in the range $[0, 1]$ to better adapt to the CNN computation dynamics.
- 2) The CNN input tensor \mathbf{z} is a realization of white gaussian noise with zero mean and standard deviation 0.1, with the same size of image \mathbf{I} . We found uniform distributions to be less effective; we are convinced the white gaussian noise is able to excite a broader frequency range and can produce better images.

- 3) We optimize the weights of the CNN through the ADAM algorithm by minimizing (9). The optimization is performed over the generator weights ϕ . Notice that the PRNU injection weight γ acts as a trainable layer of the architecture, so γ is estimated directly during the inversion. Specifically, γ is clamped to be positive, as negative γ values are not model representative.
- 4) At each minimization step, the generated image \mathbf{I}_ϕ is saved only if the PSNR with respect to the original image \mathbf{I} is above a certain threshold τ_{PSNR} . This is done in order to guarantee a sufficiently good visual quality for the generated image.

The DIP process ends when the PSNR between the generated image \mathbf{I}_ϕ and the initial image \mathbf{I} overcomes a threshold of 39dB. The maximum number of iterations is anyway fixed to 10000. In doing so, after the DIP process ends, a pool of M generated images $\mathbf{I}_\phi^{(m)}$, $m \in [1, M]$ with $\text{PSNR} \geq \tau_{\text{PSNR}}$ has been collected.

For the sake of clarity, Figs. 2 and 3 report one example of the inversion process, showing the evolution of the CNN-generated image, together with its PSNR with respect to the original image and its NCC with the source device PRNU as a function of iterations, respectively.

It is worth noticing that, although DIPPAS involves the optimization of CNN parameters, it is not trained to reconstruct a target image by learning from ground truth samples. The deep features are learnt out of the input image \mathbf{I} by minimizing the functional $J(\phi)$ in a way that can be seen as overfitting. However, DIP belongs to the context of inverse problems, where of course the modeling fits the acquired image. The main difference is that the optimization is performed in the space of the CNN parameters instead of the image space.

C. Assembly of multiple anonymized images

Notice that the minimization functional (9) imposes a constraint on the Frobenius norm of the difference between the fingerprint-injected image and the initial image. This constraint represents a global constraint as it does not specifically focus on local pixel areas. Recalling our final goals (i.e., maximizing the PSNR and minimizing the NCC of the anonymized image), while the PSNR is a global metrics as it considers the entire image and not local areas, the NCC can strongly depend on specific local regions of the image which can correlate with the device PRNU in diverse fashions.

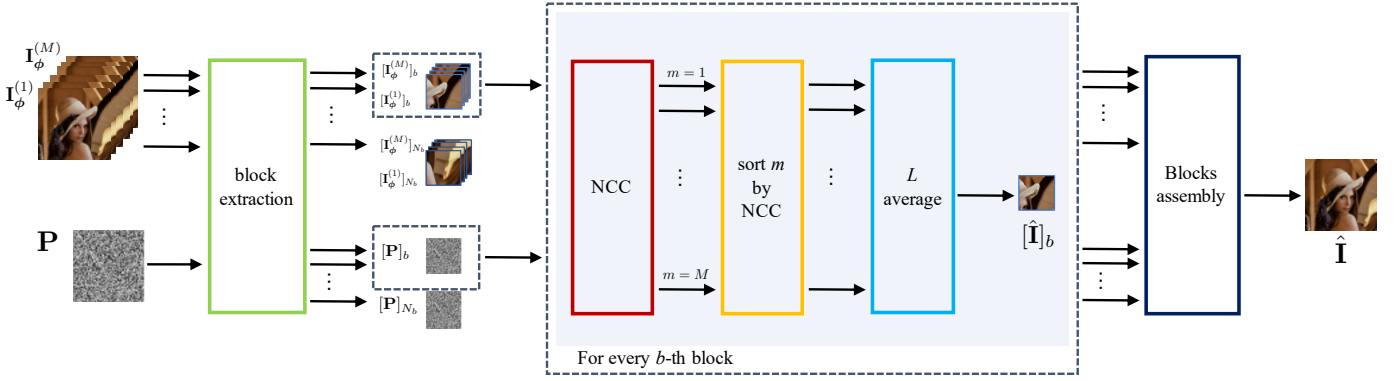


Fig. 4. Assembly of the anonymized image. For each generated image $\mathbf{I}_\phi^{(m)}$, N_b blocks are extracted from the image and the fingerprint \mathbf{P} . Fixing a block position b , we compute the NCC between each pair of blocks $[\mathbf{I}_\phi^{(m)}]_b, [\mathbf{P}]_b, m \in [1, M]$. Then, we order the M image blocks according to their resulting NCCs and we average the first L blocks pixel by pixel, obtaining the estimated block $[\hat{\mathbf{I}}]_b$. We follow this pipeline for each block position b , eventually assembling the results and estimating the anonymized image $\hat{\mathbf{I}}$.

Given these premises, we propose to further optimize our solution by investigating the M generated images on their local areas. Indeed, all the M available images represent reasonable and valuable solutions for the anonymization. However, we improve upon these results with a very simple methodology to generate one final anonymized image out of the M previously generated, by locally optimizing the cross-correlation with the reference device fingerprint \mathbf{P} .

Specifically, Fig. 4 depicts the proposed pipeline: we divide each available image $\mathbf{I}_\phi^{(m)}$ and the reference fingerprint \mathbf{P} into N_b non overlapping squared blocks of $B \times B$ pixels. Image and fingerprint blocks are defined as $[\mathbf{I}_\phi^{(m)}]_b$ and $[\mathbf{P}]_b, b \in [1, N_b]$, respectively. Notice that, for each block geometric position b , we have M available image blocks associated with the M image realizations produced during the DIPPAS iterations. For each block position b , three main steps follow:

- 1) The NCCs between the M image blocks $[\mathbf{I}_\phi^{(m)}]_b, m \in [1, M]$ and the fingerprint block $[\mathbf{P}]_b$ are computed as in (2).
- 2) The available M blocks are ordered accordingly to their resulting NCCs: first, we select the blocks with negative NCC and increasing absolute value; secondly, we select the blocks with positive NCC and increasing absolute value. In doing so, blocks with low absolute value of NCC and negative NCC are given higher priority than blocks returning bigger NCCs.
- 3) Following the order specified above, we average the first L blocks pixel by pixel, ending up with a $B \times B$ final reconstructed block.

The final anonymized image $\hat{\mathbf{I}}$ is estimated by assembling the results obtained for each single block position b and color channel.

D. CNN Architecture

The U-Net is a convolutional autoencoder (i.e., a CNN aiming at reconstructing a processed version of its input) characterized by the so called skip-connections and originally introduced for medical image processing [16]. If properly

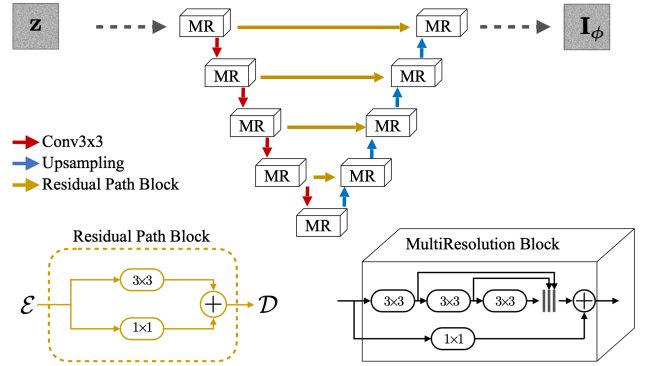


Fig. 5. Proposed Multi-Res U-Net architecture.

trained according to the standard deep learning paradigm, it proves very effective for multidimensional signal processing tasks such as denoising [30], [31], interpolation [32], [33], segmentation [34], [35], inpainting [36], and domain-specific post-processing operators [37], [38].

More recently, the MultiResUNet [15] has been proposed to improve the performance of the U-Net for multimodal medical image segmentation, based on the consideration that the targets of interest have different shapes and scales. If we want to capture self-similarities of natural images to be employed as a prior for the inverse problem, working at different scales can be strongly beneficial. Therefore, we propose an ad-hoc MultiResUNet (shown in Fig. 5) that can be summarized as follows:

- 1) Convolutional layers are replaced by so called Multi Resolution (MultiRes) blocks shown in the bottom-right portion of Fig. 5. These blocks approximate multi-scale features of the Inception block while limiting the number of parameters of the network, which is critical when employing it as a deep prior.
- 2) Skip connections, which are the distinctive feature of the U-Net, are replaced by Residual Path blocks shown in the bottom-left portion of Fig. 5. \mathcal{E} is the output of an encoding layer and \mathcal{D} is concatenated to the

corresponding decoding layer.

- 3) Downsampling is achieved by 3×3 convolutions with stride 2×2 . Upsampling is performed by nearest neighbor interpolation. Batch Normalization and LeakyReLU activation functions follow every convolution apart from the last one (responsible for the CNN output) that is activated by a sigmoid.

Notice that, even though the result is the output of a CNN, the DIP method does not exploit the typical deep learning paradigm where a training phase is performed over a specifically designed set of data. In particular, only the query image is used in the reconstruction process and the CNN implicitly assumes the role of prior information that exploits correlations in the image to learn its inner structure. Therefore, the choice of a specific CNN architecture is crucial for a suitable and well-performing solution.

IV. EXPERIMENTS

In this section, we describe the used datasets, the experimental setup and the evaluation metrics.

A. Datasets

We resort to two well-known datasets, commonly used for investigating PRNU-related problems on images. The first dataset is the Dresden Image Database [17], which collects both uncompressed and compressed images from more than 50 diverse devices. Following the same procedure done in past works proposed in literature [13], [12], we select images from 6 different camera instances, precisely Nikon D70, Nikon D70s, Nikon D200, two devices each. Second dataset is the recently released Vision Dataset [18], which includes JPEG compressed images captured from 35 devices. Among the pool of available models, we collect images from 6 different camera vendors, precisely from devices named as D12, D17, D19, D21, D24, D27 in [18].

The PRNU fingerprint of each device is computed by collecting all the available flat-field images shot by the device and following the Maximum Likelihood estimation proposed in [2]. Concerning the Dresden dataset, we exploit never-compressed Adobe Lightroom images to compute the PRNU, as it reasonably is the most accurate way to estimate the device fingerprint. Indeed, JPEG compression can create blockiness artifacts that may hinder PRNU estimation [2]. Every device includes 25 homogeneously lit flat-field images for the PRNU estimation. For Vision dataset, we have more than 95 JPEG flat-content images to compute each device fingerprint.

The images to be anonymized are selected from natural images, precisely we pick 100 natural images per device. Regarding Dresden dataset, two different sub-sets can be extracted: for every device, we select 100 never-compressed Adobe Lightroom images, together with other 100 taken from the pool of JPEG compressed images. We end up with three distinct datasets comprising 600 images each: the Dresden uncompressed dataset, called \mathcal{D}_u ; the Dresden compressed dataset, defined as \mathcal{D}_c ; the Vision (compressed) dataset, \mathcal{V} .

B. State-of-the-art solutions

As state-of-the-art solutions, we select the most recent anonymization methods proposed in literature.

Among the pool of PRNU-aware methods, we implement the method proposed in [6], being the most recent and cited contribution. We do not compare our solution with the PRNU-aware strategy recently proposed in [8], as its performance drops significantly whenever the used image denoising operator during cross-correlation tests is the commonly used one suggested in [1], [2]. Since in our proposed strategy we follow the methodology devised in [1], [2] for image denoising and cross-correlation, a comparison with [8] would be unfair.

Regarding PRNU-blind strategies, the most recent contribution is that proposed by [13], which demonstrates to outperform results of [12] in a PRNU-blind scenario. For the implementation of [13], we consider the parameter configurations achieving the best anonymization results, i.e., the strategies defined as $\ell_1^{(3)}$ and $\ell_1^{(5)}$ in the original paper.

Moreover, to show that simple denoising does not achieve good anonymization performances [10], we implement the well-known DnCNN denoiser [30] which represents a modern data-driven solution among image denoising strategies.

C. Experimental Setup

An interesting aspect of the DIP paradigm is that the CNN can process images of any size. Obviously, the bigger the input image, the heavier the computation. Indeed the computing node has to store in memory all the CNN weights. However, it is worth considering that the proposed method can also be applied in a patch-wise fashion and its parallelization is straightforward. Given these premises and considering what was done in the past state-of-the-art [13], our experiments process images of 512×512 pixels with 512 features extracted at the first MultiRes block. To do so, we center-crop all the images and the computed PRNUs to a common resolution of 512×512 pixels. The optimization is performed through ADAM algorithm with learning rate 0.001. At each iteration we perturb the CNN input noise \mathbf{z} with additive white gaussian noise with standard deviation 0.1 to strengthen the convergence. Without any specific code optimization, we reach a computation speed of 5 iterations per second on a Nvidia Tesla V100 GPU, requiring 8 GB of GPU memory.

Concerning the proposed methodology in III-C, notice that the amount of M available images at the output of DIPPAS process changes accordingly to the input image. It is worth noticing that the vast majority of images needs few iterations (less than 3000 iterations over 10000 possible cycles, on average) to achieve the threshold of 39dB chosen to quit the inversion. We consider multiple parameter configurations in order to include a sufficiently wide pool of investigation cases. The block size B can be chosen among $B = [32, 64, 128, 256, 512]$ pixels, and the maximum number of averaged blocks can vary as well, being $L = [1, 5, 10, 25, 50, 75, 100]$. Notice that the case $B = 512$ corresponds to select the full image, without dividing it into blocks. Furthermore, the configuration $\{L = 1, B = 512\}$ coincides with the absence of the local area post-processing proposed in Section III-C.

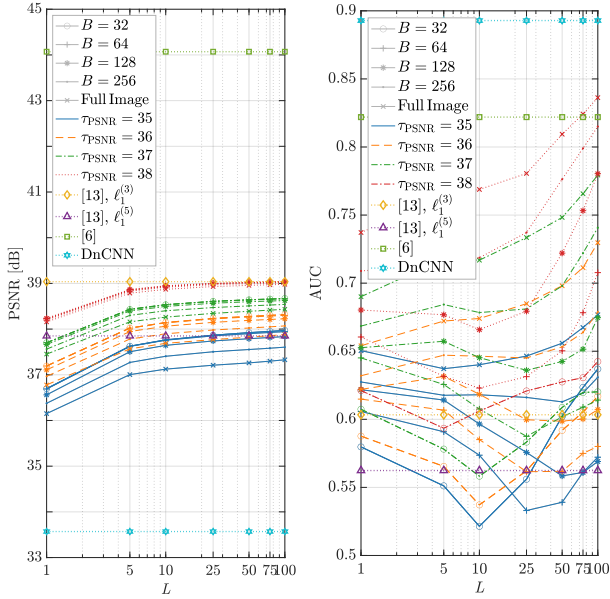


Fig. 6. PRNU-aware anonymization results for the \mathcal{D}_u dataset.

D. Evaluation Metrics

After the generation of the anonymized image $\hat{\mathbf{I}}$, we compute the NCC between $\hat{\mathbf{I}}$ and the source device PRNU \mathbf{K} , together with the PSNR between $\hat{\mathbf{I}}$ and the original image \mathbf{I} . These values are the used metrics for evaluating the results and comparing with state-of-the-art. The lower the achieved NCC together with a high PSNR, the better the image anonymization performance.

To summarize results related to the achieved NCCs, we make use of Receiver Operating Characteristic (ROC) curves related to the source device identification problem. Given a fixed device PRNU \mathbf{K} , NCCs of anonymized images taken with that device are defined as the positive set, while NCCs of images shot by other cameras are the negative set. Anonymization performance is evaluated through the Area Under the Curve (AUC), as done in [12], [13], [8]. Our goal is to reduce the AUC of the curves, thus making the PRNU-based identification not working, at the same time maintaining high values of PSNR.

V. RESULTS

In this section we provide the numerical results achieved with our experimental campaign that demonstrate the capability and limitations of our methodology. First, we deploy our method when the reference PRNU of the device is available at the analyst (i.e., $\mathbf{P} = \mathbf{K}$). Then, we show that our method can also be applied in the case of blind anonymization when the PRNU \mathbf{K} is unknown (i.e., $\mathbf{P} = \mathbf{W}$). Results are compared with state-of-the-art techniques to highlight pros and cons.

A. PRNU-aware anonymization

In this scenario, the actual PRNU of the source device to be anonymized is known. Results are shown in terms of PSNR and AUC of the ROC curves for the three investigated datasets. Figs. 6, 7, 8 refer to datasets \mathcal{D}_u , \mathcal{D}_c and \mathcal{V} , respectively.

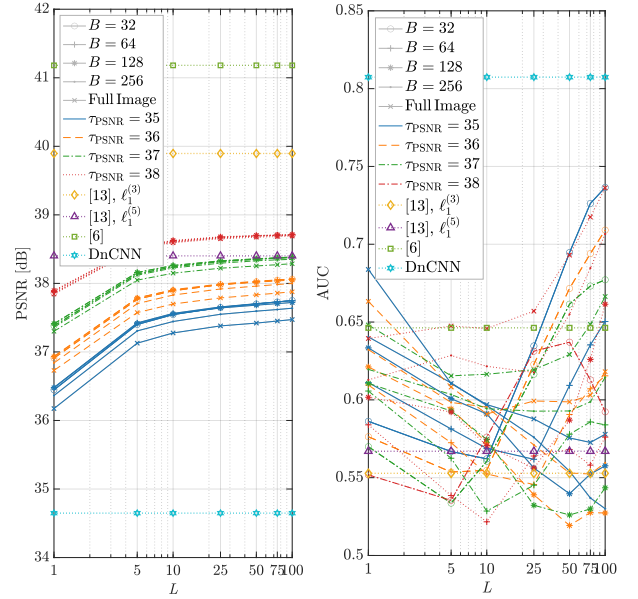


Fig. 7. PRNU-aware anonymization results for the \mathcal{D}_c dataset.

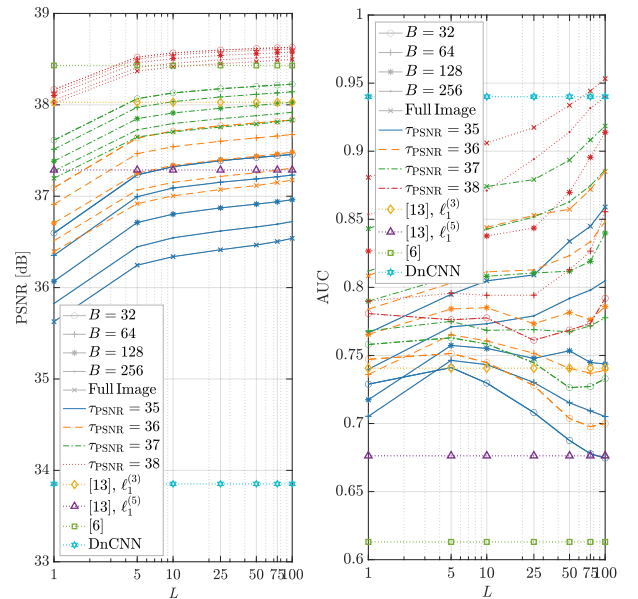


Fig. 8. PRNU-aware anonymization results for the \mathcal{V} dataset.

It is important to notice that results must be analyzed by watching PSNR and AUC concurrently. Indeed, high PSNR is a good result only if paired with low AUC. We therefore privilege solutions providing a good PSNR / AUC trade-off. To ease the readability of reported results, we separately analyze in brief paragraphs the performance of each PRNU-anonymization method.

Proposed DIPPAS method. For all the investigated datasets, the proposed method is able to achieve PSNRs greater than 38 dB, provided that a sufficiently high threshold τ_{PSNR} is chosen. In general, the smaller the block size B , the better the PSNR achieved by the proposed method, even though this behaviour seems to attenuate for high values of τ_{PSNR} . Besides, the more the amount of averaged blocks L , the better the achieved

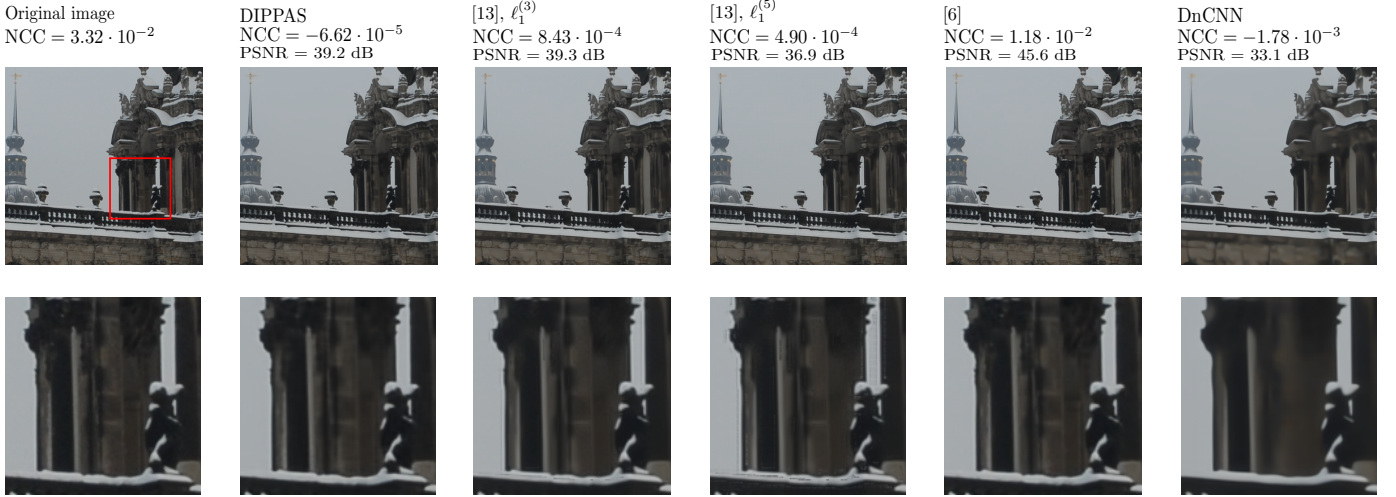


Fig. 9. PRNU-aware anonymization for an image of the \mathcal{D}_c dataset, comparing our proposed strategy with [13], [6] and DnCNN.

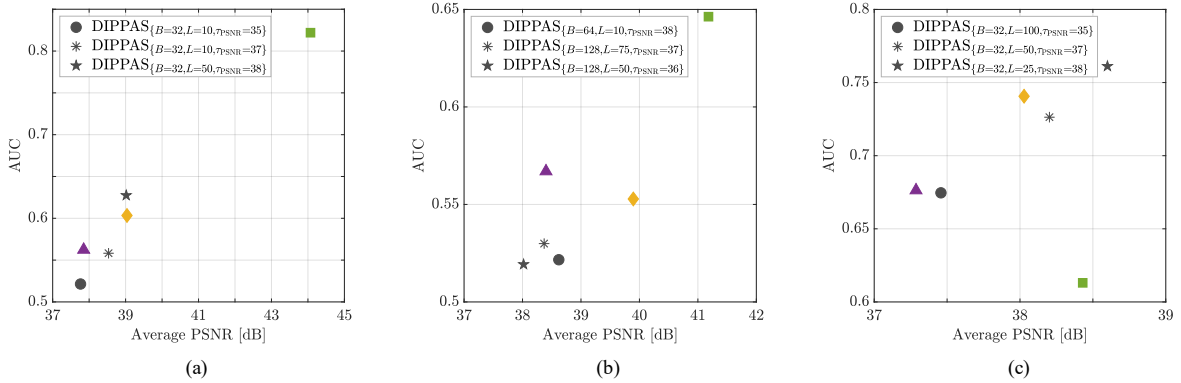


Fig. 10. PRNU-aware anonymization results, reported in terms of AUC as a function of average PSNR achieved by three DIPPAS configurations for (a): the \mathcal{D}_u dataset, (b): the \mathcal{D}_c dataset, (c): the \mathcal{V} dataset. We compare our proposed strategy with [13] $\ell_1^{(3)}$ (yellow \diamond), [13] $\ell_1^{(5)}$ (purple \triangle) and [6] (green \blacksquare).

PSNR. In terms of AUCs, the proposed method can cover a wide range of possibilities, according to the chosen block size B and amount of averaged blocks L . Regarding Dresden-related datasets, middle values of L seem to work better for achieving good AUCs, while dataset \mathcal{V} requires higher values of L for lowering the AUC. The achieved AUCs are better on Dresden-related datasets, i.e., Figs. 6 and 7. For these two datasets, none of the state-of-the-art works outperforms the best DIPPAS results, while \mathcal{V} dataset seems to be more challenging to be anonymized.

Proposed method in [6]. The solution provided by [6] achieves the best results in terms of PSNR for all three datasets. However, notice that the corresponding AUCs show very poor results if compared with DIPPAS and [13] for Dresden-related datasets. Concerning the dataset \mathcal{V} shown in Fig. 8, the AUC obtained by [6] seems to outperform every proposed strategy. We think this different behaviour can be explained by the diverse nature of Vision dataset with respect to Dresden. Indeed, in dataset \mathcal{V} the device PRNU is estimated directly from JPEG-compressed images, while in Dresden-based datasets the PRNU is estimated from uncompressed ones. As a matter of fact, the PRNU estimated from JPEG-compressed images can present artifacts due to

JPEG compression, which can also contribute to hinder the subtle sensor traces left on images [2]. As a consequence, anonymizing JPEG-compressed images with respect to the PRNU estimated from uncompressed data can be slightly more complicated than anonymizing JPEG images with respect to the PRNU estimated from JPEG data. In this vein, the strategy proposed by [6] seems to work in a very accurate way only if the device PRNU is estimated from JPEG-compressed images. **Proposed method in [13].** The proposed strategy in [13] achieves acceptable values of PSNRs in all the considered datasets, actually comparable to those achieved by DIPPAS. The resulting AUCs show satisfying values as well, except for the Vision-related dataset, where [13] seems to suffer more with respect to Dresden-related datasets, following a similar trend to that previously shown by DIPPAS method. Regardless, notice that DIPPAS can outperform the AUCs achieved by [13] in all three datasets.

Proposed method in [30]. The DnCNN solution proposed in [30] shows small values of PSNRs in all the experiments. Furthermore, the achieved results report too high AUCs, actually unacceptable for satisfactory image anonymization. DnCNN results seem to confirm that image denoising cannot accurately delete PRNU traces [10], leading to poor anonymization

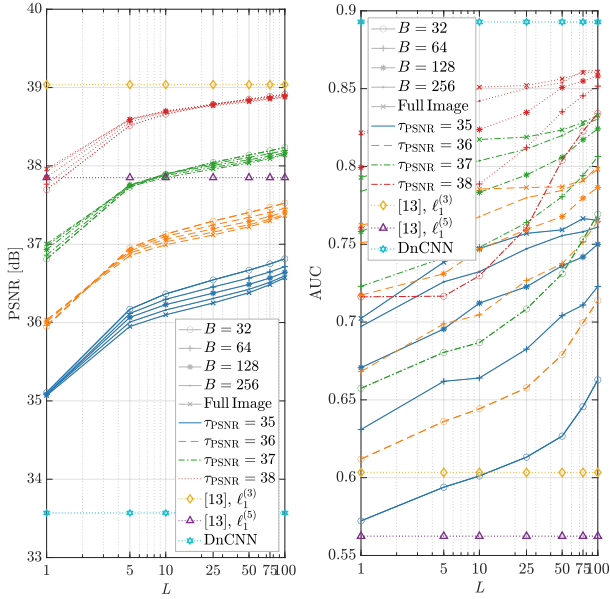


Fig. 11. PRNU-blind anonymization results for the \mathcal{D}_u dataset.

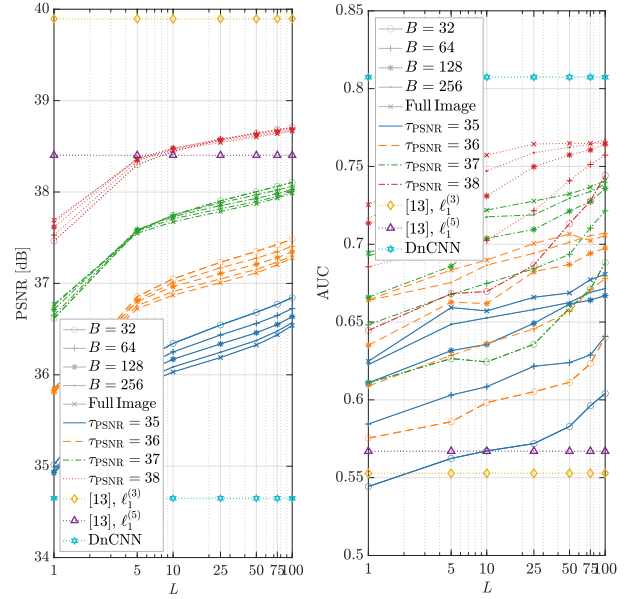


Fig. 12. PRNU-blind anonymization results for the \mathcal{D}_c dataset.

performances.

For the sake of clarity, Fig. 9 reports an example of anonymization performed over an image of \mathcal{D}_c dataset. We depict the original image and its anonymized versions exploiting DIPPAS and the methods of [13], [6] and DnCNN [30], respectively. Specifically, we choose the best performing DIPPAS parameter configuration in terms of both PSNR and AUC, i.e., $\{\tau_{\text{PSNR}} = 38, B = 64, L = 10\}$; we select this configuration by referring to results shown in Fig. 7. Zooming in the images (red squared area), we can visually notice that the best results are obtained by DIPPAS and [6]; DnCNN results in a heavily smoothed image, while [13] introduces some edge artifacts. The method devised in [6] is able to halve the original NCC, while DIPPAS dramatically scales the original NCC value by a factor of 0.002.

To summarize the previously reported results, Fig. 10 shows the behaviour of AUC as a function of the average PSNR achieved by DIPPAS in three selected parameter configurations. We compare our results with state-of-the-art as well. The best working condition consists in high PSNR and low AUC. It is possible to notice that DIPPAS provides the best trade-off on Dresden dataset, and the second best one on Vision.

B. PRNU-blind anonymization

In this scenario, the actual device PRNU is unknown, therefore the reference device fingerprint used during the DIP inversion and the blocks assembly corresponds to the noise residual extracted from the image, i.e., $\mathbf{P} = \mathbf{W}$. As previously done, we report the PSNR and AUC of the ROC curves for all three investigated datasets. Figs. 11, 12, 13 depicts results for datasets \mathcal{D}_u , \mathcal{D}_c and \mathcal{V} , respectively.

In terms of PSNRs, on Vision dataset we are able to outperform [13], while for Dresden-related datasets we achieve slightly lower results. Moreover, DIPPAS achieves slightly higher AUCs than state-of-the-art solutions. Notice that the

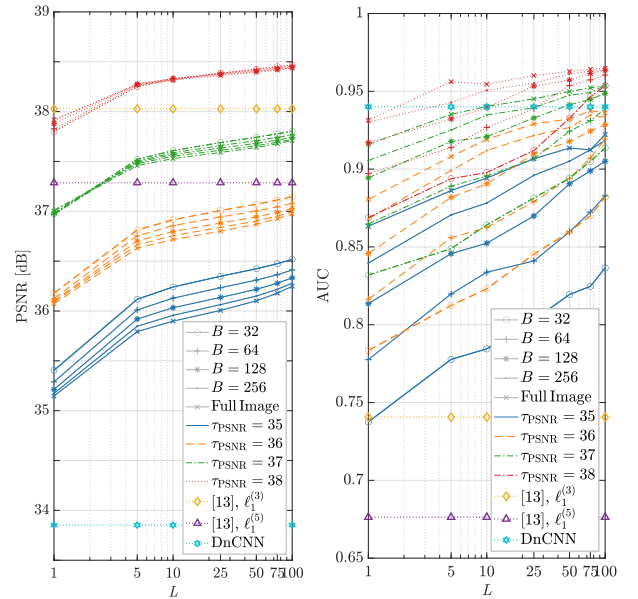


Fig. 13. PRNU-blind anonymization results for the \mathcal{V} dataset.

best AUC values are obtained for $L = 1$, i.e., without performing block averaging.

We think this less effective anonymization with respect to the previous PRNU-aware scenario can be due to the assumption done during the DIPPAS inversion (9) in order to estimate the anonymized image. As a matter of fact, the DIPPAS paradigm leverages the PRNU-based image modeling reported in (1). Whenever the PRNU estimate \mathbf{K} is unknown and the noise residual \mathbf{W} is used instead, as reported in (11), the model is not clearly satisfied and the DIPPAS solution will be sub-optimum. For this reason, in a PRNU-blind scenario, DIPPAS is still able to achieve good accuracies in terms of PSNR, however failing against the method [13] for what concerns the AUCs.

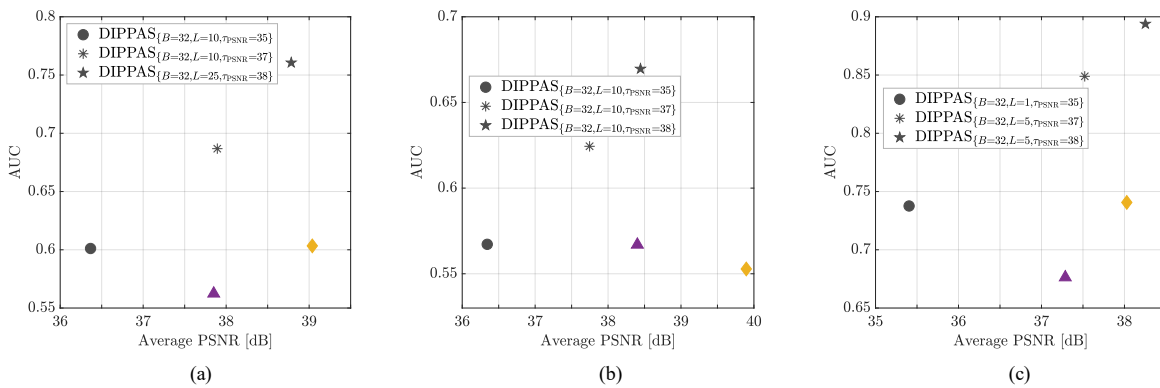


Fig. 14. PRNU-blind anonymization results, reported in terms of AUC as a function of average PSNR achieved by three DIPPAS configurations, for (a): the \mathcal{D}_u dataset, (b): the \mathcal{D}_c dataset, (c): the \mathcal{V} dataset, comparing our proposed strategy with [13] $\ell_1^{(3)}$ (yellow \diamond) and [13] $\ell_1^{(5)}$ (purple \triangle).

Following the same reasoning previously done for the PRNU-aware scenario, we show in Fig. 14 the AUC behaviour as a function of the average PSNR, selecting three diverse DIPPAS parameter configurations for each dataset. From these results it seems that DIPPAS cannot achieve better results than [13], but an important point has to be noticed. Indeed, [13] applies different processing to edges and to flat regions, thus removing PRNU traces in concentrated local regions. In the next subsection we investigate the effect of this choice.

C. Comparison with [13] along image edges

Since method [13] outperforms our PRNU-blind proposed solution in the majority of cases, we propose a further analysis in order to carefully compare the two strategies. Precisely, notice that method [13] works in two separate steps: (i) estimate an anonymized version of the image exploiting inpainting techniques; (ii) substitute a denoised version of the edges extracted from the original image into the anonymized image, in order to enhance the output visual quality. In light of these considerations, we think that the edge processing operation performed on the output image can be the weak link in the proposed pipeline of [13]. Indeed, image edges only undergo two successive steps of BM3D denoising algorithm [39], thus they reasonably contain enough PRNU traces for performing source attribution, as suggested in [10].

Therefore, we propose to compare DIPPAS and [13] only along the image edges, extracted following the same pipeline proposed in [13]. For every dataset, we evaluate DIPPAS results for a parameter configuration which returns the nearest PSNR value to that achieved by [13]. For instance, looking at Fig. 11, dataset \mathcal{D}_u is evaluated for $\{B = 32, L = 100, \tau_{\text{PSNR}} = 38\}$ if compared to [13], $\ell_1^{(3)}$; we use $\{B = 512, L = 10, \tau_{\text{PSNR}} = 37\}$ when comparing to [13], $\ell_1^{(5)}$.

We compare results in terms of relative change of AUC evaluated over image edges with respect to the AUC achieved on the full image. In a nutshell, the relative change in AUC can be computed as $(\text{AUC}_{\text{edges}} - \text{AUC})/\text{AUC}$, being AUC the metrics associated to the full image. Table I reports the results. Notice that the relative AUC change maintains a coherent behaviour for all the three datasets. On one side, [13] always

TABLE I
AUC RELATIVE CHANGE ON IMAGE EDGES, FOR PRNU-BLIND ANONYMIZATION.

NCC area	[13], $\ell_1^{(3)}$	DIPPAS	NCC area	[13], $\ell_1^{(5)}$	DIPPAS
$\mathcal{V}_{\text{edges}}$	+11.6%	-9.1%	$\mathcal{V}_{\text{edges}}$	+22.3%	-9.9%
$\mathcal{D}_u_{\text{edges}}$	+10.9%	-17.8%	$\mathcal{D}_u_{\text{edges}}$	+19.1%	-19.1%
$\mathcal{D}_c_{\text{edges}}$	+8.7%	-17.6%	$\mathcal{D}_c_{\text{edges}}$	+6.1%	-17.7%

reports a positive relative change; on the other side, DIPPAS presents a negative relative change.

DIPPAS results emulate what actually happens on natural images when compared with the PRNU in a reduced region (e.g., only along the edges). Indeed, the NCC drops as the image content is reduced, thus the AUC of the source attribution problem decreases. On the contrary, accuracy of [13] evaluated only along image edges strongly drops as the NCC increases, with a consequent AUC growth. This phenomenon can be explained by the previously reported consideration, that is, [13] performs only denoising along the edges and this is usually not enough to hinder PRNU traces [10]. As a consequence, the anonymization algorithm proposed in [13] can be easily spotted and defeated just by analyzing image edges, whereas the DIPPAS proposed solution does not present this drawback. Even if an analyst only use edges for PRNU-based attribution, the image would look anonymized.

VI. CONCLUSIONS

In this manuscript, we propose a source device anonymization scheme that leverages Deep Image Prior (DIP) paradigm to attenuate PRNU traces in natural images. With this method, a CNN learns to generate a PRNU-free image starting from a noise realization. Specifically: (i) the CNN generates an image; (ii) we inject the device PRNU into this image; (iii) we minimize the distance between the input query image and the PRNU-injected image. In doing so, we are able to generate an anonymized image with a strongly attenuated PRNU pattern and high visual quality.

To this purpose, we define the PRNU anonymization task as an inverse problem. Then we recast such problem as a DIP problem, finding the CNN parameters that produce the

best estimate of the PRNU-free image. Finally, we devise a post-processing operator for assembling the final anonymized image from the CNN outputs realized at different iterations.

We compare our method against state-of-the-art anonymization schemes through numerical examples. In particular, when the PRNU of the device is available, we achieve our best results. Our scheme can be generalized to the case of blind anonymization, i.e., when the device PRNU is unknown and only a noise residual can be extracted from the query image and then injected into the CNN output image.

Not surprisingly, our method suffers when the injected noise is quite different from the source device PRNU. However, it still proves superior to the considered state-of-the-art counterpart if we consider the homogeneity of PRNU removal effect. Indeed, we are capable of removing PRNU traces on all image regions, whereas the considered baseline mainly leaves image edges non-anonymized.

Our future work will be devoted to investigate the possibility of starting from a pre-trained network to speed-up convergence. Moreover we will focus on a better inversion model to be used in case of blind PRNU removal.

REFERENCES

- [1] J. Lukáš, J. Fridrich, and M. Goljan, "Digital camera identification from sensor pattern noise," *IEEE Transactions on Information Forensics and Security (TIFS)*, vol. 1, pp. 205–214, 2006.
- [2] M. Chen, J. Fridrich, M. Goljan, and J. Lukas, "Determining image origin and integrity using sensor noise," *IEEE Transactions on Information Forensics and Security (TIFS)*, vol. 3, pp. 74–90, 2008.
- [3] M. Kirchner and C. Johnson, "SPN-CNN: Boosting Sensor-Based Source Camera Attribution with Deep Learning," in *IEEE International Workshop on Information Forensics and Security*, December 2019.
- [4] S. Mandelli, D. Cozzolino, P. Bestagini, L. Verdoliva, and S. Tubaro, "Cnn-based fast source device identification," *IEEE Signal Processing Letters*, vol. 27, pp. 1285–1289, 2020.
- [5] M. Chen, J. Fridrich, M. Goljan, and J. Lukas, "Source digital camcorder identification using sensor photo-response nonuniformity," in *SPIE Electronic Imaging (EI)*, 2007.
- [6] A. Karaküçük and A. E. Dirik, "Adaptive photo-response non-uniformity noise removal against image source attribution," *Journal of Digital Investigation*, vol. 12, pp. 66–76, 2015.
- [7] H. Zeng, J. Chen, X. Kang, and W. Zeng, "Removing camera fingerprint to disguise photograph source," in *IEEE International Conference on Image Processing (ICIP)*, 2015.
- [8] N. Bonettini, L. Bondi, D. Güera, S. Mandelli, P. Bestagini, S. Tubaro, and E. J. Delp, "Fooling prnu-based detectors through convolutional neural networks," in *2018 26th European Signal Processing Conference (EUSIPCO)*. IEEE, 2018, pp. 957–961.
- [9] K. Rosenfeld and H. T. Sencar, "A study of the robustness of PRNU-based camera identification," in *IS&T/SPIE Electronic Imaging (EI)*. International Society for Optics and Photonics, 2009.
- [10] J. Bernacki, "On robustness of camera identification algorithms," *Multimedia Tools and Applications*, pp. 1–22, 2020.
- [11] A. E. Dirik, H. T. Sencar, and N. Memon, "Analysis of seam-carving-based anonymization of images against PRNU noise pattern-based source attribution," *IEEE Transactions on Information Forensics and Security (TIFS)*, vol. 9, pp. 2277–2290, 2014.
- [12] J. Entrieri and M. Kirchner, "Patch-based desynchronization of digital camera sensor fingerprints," in *IS&T Electronic Imaging (EI)*, 2016.
- [13] S. Mandelli, L. Bondi, S. Lameri, V. Lipari, P. Bestagini, and S. Tubaro, "Inpainting-based camera anonymization," in *IEEE International Conference on Image Processing (ICIP)*, 2017.
- [14] D. Ulyanov, A. Vedaldi, and V. Lempitsky, "Deep image prior," in *The IEEE Conference on Computer Vision and Pattern Recognition (CVPR)*, June 2018.
- [15] N. Ibtehaz and M. S. Rahman, "Multiresunet: Rethinking the u-net architecture for multimodal biomedical image segmentation," *Neural Networks*, vol. 121, pp. 74–87, 2020.
- [16] O. Ronneberger, P. Fischer, and T. Brox, "U-net: Convolutional networks for biomedical image segmentation," in *International Conference on Medical image computing and computer-assisted intervention*. Springer, 2015, pp. 234–241.
- [17] T. Gloe and R. Böhme, "The dresden image database for benchmarking digital image forensics," *Journal of Digital Forensic Practice*, vol. 3, pp. 150–159, 2010.
- [18] D. Shullani, M. Fontani, M. Iuliani, O. A. Shaya, and A. Piva, "Vision: a video and image dataset for source identification," *EURASIP Journal on Information Security*, vol. 15, 2017.
- [19] P. Moulin and Juan Liu, "Analysis of multiresolution image denoising schemes using generalized gaussian and complexity priors," *IEEE Transactions on Information Theory*, vol. 45, no. 3, pp. 909–919, 1999.
- [20] A. N. Tikhonov and V. Y. Arsenin, *Solution of Ill-Posed Problems*. V. H. Winston, 1977.
- [21] L. I. Rudin, S. Osher, and E. Fatemi, "Nonlinear total variation based noise removal algorithms," *Physica D*, vol. 60, pp. 259–268, 1992.
- [22] M. Malfait and D. Roose, "Wavelet-based image denoising using a markov random field a priori model," *IEEE Transactions on Image Processing*, vol. 6, no. 4, pp. 549–565, 1997.
- [23] Jean-Luc Starck, E. J. Candes, and D. L. Donoho, "The curvelet transform for image denoising," *IEEE Transactions on Image Processing*, vol. 11, no. 6, pp. 670–684, 2002.
- [24] M. N. Do and M. Vetterli, "The contourlet transform: an efficient directional multiresolution image representation," *IEEE Transactions on Image Processing*, vol. 14, no. 12, pp. 3089–3101, 2005.
- [25] K. Guo and D. Labate, "Optimally sparse multidimensional representation using shearlets," *SIAM Journal on Mathematical Analysis*, vol. 39, no. 1, pp. 298–318, 2007.
- [26] T. Tirer and R. Giryes, "Back-projection based fidelity term for ill-posed linear inverse problems," *IEEE Transactions on Image Processing*, vol. 29, pp. 6164–6179, 2020.
- [27] W. Dong, P. Wang, W. Yin, G. Shi, F. Wu, and X. Lu, "Denoising prior driven deep neural network for image restoration," *IEEE Transactions on Pattern Analysis and Machine Intelligence*, vol. 41, no. 10, pp. 2305–2318, 2019.
- [28] B. Lin, X. Tao, and J. Lu, "Hyperspectral image denoising via matrix factorization and deep prior regularization," *IEEE Transactions on Image Processing*, vol. 29, pp. 565–578, 2020.
- [29] H. K. Aggarwal, M. P. Mani, and M. Jacob, "Modl: Model-based deep learning architecture for inverse problems," *IEEE Transactions on Medical Imaging*, vol. 38, no. 2, pp. 394–405, 2019.
- [30] K. Zhang, W. Zuo, Y. Chen, D. Meng, and L. Zhang, "Beyond a gaussian denoiser: Residual learning of deep cnn for image denoising," *IEEE Transactions on Image Processing (TIP)*, vol. 26, no. 7, pp. 3142–3155, 2017.
- [31] C. Cruz, A. Foi, V. Katkovnik, and K. Egiazarian, "Nonlocality-reinforced convolutional neural networks for image denoising," *IEEE Signal Processing Letters*, vol. 25, no. 8, pp. 1216–1220, 2018.
- [32] F. Kong, F. Picetti, V. Lipari, P. Bestagini, and S. Tubaro, "Deep prior-based seismic data interpolation via multi-res u-net," in *SEG Technical Program Expanded Abstracts 2020*, 2020, pp. 3159–3163.
- [33] S. Mandelli, F. Borra, V. Lipari, P. Bestagini, A. Sarti, and S. Tubaro, "Seismic data interpolation through convolutional autoencoder," in *SEG Technical Program Expanded Abstracts 2018*, 2018, pp. 4101–4105.
- [34] Z. Zhou, M. M. R. Siddiquee, N. Tajbakhsh, and J. Liang, "Unet++: Redesigning skip connections to exploit multiscale features in image segmentation," *IEEE Transactions on Medical Imaging*, vol. 39, no. 6, pp. 1856–1867, 2020.
- [35] R. E. Jurdi, C. Petitjean, P. Honeine, and F. Abdallah, "Bb-unet: U-net with bounding box prior," *IEEE Journal of Selected Topics in Signal Processing*, vol. 14, no. 6, pp. 1189–1198, 2020.
- [36] O. Sidorov and J. Y. Hardeberg, "Deep hyperspectral prior: Single-image denoising, inpainting, super-resolution," in *2019 IEEE/CVF International Conference on Computer Vision Workshop (ICCVW)*, 2019, pp. 3844–3851.
- [37] F. Picetti, V. Lipari, P. Bestagini, and S. Tubaro, "Seismic image processing through the generative adversarial network," *Interpretation*, vol. 7, no. 3, pp. SF15–SF26, 2019.
- [38] F. Devoti, C. Parera, A. Lieto, D. Moro, V. Lipari, P. Bestagini, and S. Tubaro, "Wavefield compression for seismic imaging via convolutional neural networks," in *SEG Technical Program Expanded Abstracts 2019*, 2019, pp. 2227–2231.
- [39] K. Dabov, A. Foi, V. Katkovnik, and K. Egiazarian, "Image denoising by sparse 3D transform-domain collaborative filtering," *IEEE Transactions on Image Processing (TIP)*, vol. 16, pp. 2080–2095, 2007.